PCCP

Physical Chemistry Chemical Physics

ROYAL SOCIETY
OF CHEMISTRY

PAPER
Hiroshi Irie *et al.*
A heterojunction photocatalyst composed of zinc rhodium oxide, single crystal-derived bismuth vanadium oxide, and silver for overall pure-water splitting under visible light up to 740 nm

175 YEARS

A heterojunction photocatalyst composed of zinc rhodium oxide, single crystal-derived bismuth vanadium oxide, and silver for overall pure-water splitting under visible light up to 740 nm†

Ryoya Kobayashi,[a] Toshihiro Takashima,[b] Satoshi Tanigawa,[a] Shugo Takeuchi,[c] Bunsho Ohtani[d] and Hiroshi Irie*[bd]

We recently reported the synthesis of a solid-state heterojunction photocatalyst consisting of zinc rhodium oxide ($ZnRh_2O_4$) and bismuth vanadium oxide ($Bi_4V_2O_{11}$), which functioned as hydrogen (H_2) and oxygen (O_2) evolution photocatalysts, respectively, connected with silver (Ag). Polycrystalline $Bi_4V_2O_{11}$ (p-$Bi_4V_2O_{11}$) powders were utilized to form $ZnRh_2O_4$/Ag/p-$Bi_4V_2O_{11}$, which was able to photocatalyze overall pure-water splitting under red-light irradiation with a wavelength of 700 nm (R. Kobayashi *et al.*, *J. Mater. Chem. A*, 2016, **4**, 3061). In the present study, we replaced p-$Bi_4V_2O_{11}$ with a powder obtained by pulverizing single crystals of $Bi_4V_2O_{11}$ (s-$Bi_4V_2O_{11}$) to form $ZnRh_2O_4$/Ag/s-$Bi_4V_2O_{11}$, and demonstrated that this heterojunction photocatalyst had enhanced water-splitting activity. In addition, $ZnRh_2O_4$/Ag/s-$Bi_4V_2O_{11}$ was able to utilize nearly the entire range of visible light up to a wavelength of 740 nm. These properties were attributable to the higher O_2 evolution activity of s-$Bi_4V_2O_{11}$.

Introduction

Since the first report of photo-induced water splitting by titanium dioxide (TiO_2) and platinum (Pt) electrodes,[1] the potential to convert photon energy into hydrogen (H_2) energy by photo-catalytic water-splitting using photoelectrodes and powdered photocatalysts has been extensively investigated due to the simplicity of the process and the possibility for large-scale H_2 production. Numerous studies have attempted to identify powdered photocatalysts that are able to split water into H_2 and oxygen (O_2) at a molar ratio of $\sim 2:1$ (overall water splitting),[2–26] particularly under visible-light irradiation for the efficient utilization of sunlight energy.[8–26] One of the major approaches for overall water splitting is the construction of "Z-scheme" systems, which are composed of two visible-light sensitive photocatalysts. These systems were first reported by Sayama and coworkers, who used Pt-deposited strontium titanate co-doped

with chromium and tantalum (Pt/SrTiO₃:Cr,Ta) as an H_2 evolution photocatalyst (H_2 photocatalyst) and Pt-deposited tungsten trioxide (Pt/WO₃) as an O_2 evolution photocatalyst (O_2 photocatalyst).[20] To date, numerous Z-scheme systems consisting of various H_2 and O_2 photocatalysts have been reported.[21–23]

Despite the potential of Z-scheme systems for photocatalytic water splitting, most systems reported to date are only able to utilize visible light up to a wavelength of 520 nm. In addition, because conventional Z-scheme systems require a suitable redox mediator, such as iodate (IO_3^-)/iodide (I^-) or ferric (Fe^{3+})/ferrous (Fe^{2+}) ions, these systems are not capable of splitting "pure" water (*i.e.*, distilled water without chemicals). Recently, solid-state Z-scheme systems that function in the absence of a redox mediator have been reported.[24,25] However, because the pH of the system required adjustment to 3.5 using sulfuric acid (H_2SO_4), pure-water splitting was not accomplished.

Recently, we developed novel solid-state photocatalysts by inserting silver (Ag) as an electron mediator between zinc rhodium oxide ($ZnRh_2O_4$, E_g of 1.2 eV) as an H_2 photocatalyst and defective silver antimonate ($Ag_{1-x}SbO_{3-y}$, E_g of 2.7 eV) or bismuth vanadium oxide ($Bi_4V_2O_{11}$) as an O_2 photocatalyst ($ZnRh_2O_4$/Ag/$Ag_{1-x}SbO_{3-y}$[26] or $ZnRh_2O_4$/Ag/$Bi_4V_2O_{11}$[27]). Using these systems, overall pure-water splitting proceeded *via* the inserted Ag, which mediated the transfer of photoexcited electrons from the conduction band (CB) of the O_2 photocatalyst to the valence band (VB) of the H_2 photocatalyst. $ZnRh_2O_4$/Ag/$Ag_{1-x}SbO_{3-y}$ and $ZnRh_2O_4$/Ag/$Bi_4V_2O_{11}$ utilized visible light up

a Special Doctoral Program for Green Energy Conversion Science and Technology, Interdisciplinary Graduate School of Medicine and Engineering, University of Yamanashi, 4-3-11 Takeda, Kofu, Yamanashi 400-8511, Japan

b Clean Energy Research Center, University of Yamanashi, 4-3-11 Takeda, Kofu, Yamanashi 400-8511, Japan. E-mail: hirie@yamanashi.ac.jp

c Graduate School of Environmental Science, Hokkaido University, Nishi 10, Nishi 5, Sapporo, Hokkaido 060-0810, Japan

d Institute for Catalysis, Hokkaido University, Nishi 10, Kita 21, Sapporo, Hokkaido 001-0021, Japan

† Electronic supplementary information (ESI) available. See DOI: 10.1039/c6cp02903e

27754 | *Phys. Chem. Chem. Phys.*, 2016, **18**, 27754–27760

This journal is © the Owner Societies 2016

to wavelengths of 545 and 700 nm, respectively, a property that was determined by the photoactivity of $Ag_{1-x}SbO_{3-y}$ and $Bi_4V_2O_{11}$. In the previous study, we utilized polycrystalline $Bi_4V_2O_{11}$ (p-$Bi_4V_2O_{11}$) powder, which was prepared by a normal solid-state reaction, for the synthesis of $ZnRh_2O_4/Ag/Bi_4V_2O_{11}$.

In the present study, $Bi_4V_2O_{11}$ powder was obtained by pulverizing single crystals of $Bi_4V_2O_{11}$ (s-$Bi_4V_2O_{11}$) to form the powdered photocatalyst $ZnRh_2O_4/Ag/s-Bi_4V_2O_{11}$, which displayed enhanced water-splitting activity compared to $ZnRh_2O_4/Ag/p-Bi_4V_2O_{11}$. Notably, $ZnRh_2O_4/Ag/s-Bi_4V_2O_{11}$ was able to utilize visible light up to wavelengths of 740 nm, which represents nearly the entire visible light spectrum and to our knowledge, is the longest wavelength reported to date (ESI 1†).

Experimental

Sample preparation

A melting–slow cooling method was applied to grow single crystals of $Bi_4V_2O_{11}$ (s-$Bi_4V_2O_{11}$) by melting (940 °C) and slow cooling (4 °C h^{-1} to 740 °C) of stoichiometric mixtures of commercial bismuth oxide (Bi_2O_3, purity 99.9%; Kanto Kagaku) and vanadium oxide (V_2O_5, purity 99.0%; Kanto Kagaku) powders.[28] The obtained single crystals adopted a thin plate-like sheet structure and had a thickness of ~0.2 mm and transverse dimensions of ~1 mm × 2 mm. The thin sheets of $Bi_4V_2O_{11}$ were used directly for Laue photography and X-ray diffractometer analyses, and were further pulverized for use in all other experiments.

$ZnRh_2O_4$ powders were synthesized using a solid-state reaction method. Briefly, stoichiometric amounts of commercial zinc oxide (ZnO, purity 99.0%; Kanto Kagaku) and rhodium oxide (Rh_2O_3, purity 99.9%; Kanto Kagaku) powders were mixed and calcined at 1000 °C for 24 h and the obtained powders were thoroughly ground. As a reference, the Bi_2O_3 and V_2O_5 powders were mixed and calcined at 850 °C for 8 h to prepare poly-crystal powders of $Bi_4V_2O_{11}$ (p-$Bi_4V_2O_{11}$), which were thoroughly ground prior to experimental use.

A powdered heterojunction photocatalyst composed of $ZnRh_2O_4$, s-$Bi_4V_2O_{11}$, and Ag ($ZnRh_2O_4/Ag/s-Bi_4V_2O_{11}$) was prepared using the following simple method.[27] $ZnRh_2O_4$, Ag_2O, and s-$Bi_4V_2O_{11}$ powders were mixed at a molar ratio of 1:1:1.2 in an identical manner to that described above. The mixed powders were pressed into pellets by applying a force of 60 kN, and the pellets were then heated at 750 °C for 2 h. The pellets were ground into a fine powder, which was soaked in an aqueous solution (50 mL) of 3 M nitric acid (HNO_3, Kanto Kagaku) for 15 min. The powder was filtered and thoroughly washed with distilled water, and was then dried at 65 °C for 12 h. As a reference, $ZnRh_2O_4/Ag/p-Bi_4V_2O_{11}$ was also prepared using the same procedure.[27]

Characterization

A Laue camera (SA-HFM3, Rigaku) was used for the characterization of $Bi_4V_2O_{11}$ single crystals. The crystal structures of the single crystals and powder obtained by pulverizing single crystals were determined by X-ray diffraction (XRD) using a PW-1700 X-ray diffractometer (PANalytical). The structure of the $ZnRh_2O_4/Ag/Bi_4V_2O_{11}$ powder was also determined by XRD. The Brunauer–Emmett–Teller (BET) surface area was determined using a nitrogen adsorption apparatus (Micromeritics, TriStar 3000, Shimadzu). UV-visible absorption (UV-vis) spectra were obtained by the diffuse reflection method using a V-650 spectrometer (Jasco) with barium sulfate ($BaSO_4$) as the reflectance standard. Photoacoustic (PA) spectroscopy measurements were conducted in a nitrogen atmosphere under monochromic light generated from a 300 W xenon (Xe) lamp (LX300, Eagle) equipped with a monochromator (CT-101T, Jasco) and modulated by a light chopper at 80 Hz. The PA signal was amplified and monitored using a digital lock-in amplifier (LI5640, NF).[29,30] A scanning electron microscope (SEM, JSM-6500F, JEOL Ltd) was used to observe the morphology of the prepared photocatalysts. A scanning transmission electron microscope (STEM, Tecnai Osiris, FEI) was also utilized with element maps obtained by energy-dispersive X-ray spectrometry (EDS).

O_2 evolution activity by the half reaction of water

Action spectra for O_2 evolution were measured in 3 mL water containing either s-$Bi_4V_2O_{11}$ or p-$Bi_4V_2O_{11}$ powder (30 mg) and Ce^{4+} (cerium sulfate ($Ce(SO_4)_2$), 0.1 mol L^{-1}; Kanto Kagaku) as a sacrificial agent. The pH of the solution was not adjusted prior to the spectral measurements, which were performed with constant stirring using a magnetic stirrer and under illumination with monochromatic light (570 ± 5 to 750 ± 5 nm) generated from a diffraction grating-type illuminator (CRM-FD, Jasco) equipped with a 300 W Xe lamp (C2578-02, Hamamatsu Photonics). Higher-order diffracted light was cut off using an appropriate glass filter. The amount of evolved O_2 was monitored using a gas chromatograph (GC-8A, Shimadzu). The wavelength dependence of the AQE was then evaluated. AQE values for O_2 evolution were calculated using the equation: AQE (%) = 100 × 4 × O_2 evolution rate/incident photon rate, because O_2 evolution is represented by the formula: $2H_2O + 4h^+ \rightarrow O_2 + 4H^+$.

Water-splitting reactions

To evaluate the photocatalytic activity, $ZnRh_2O_4/Ag/s-Bi_4V_2O_{11}$ or $ZnRh_2O_4/Ag/p-Bi_4V_2O_{11}$ composite powder (60 mg) was suspended in 12 mL pure water (pH unadjusted) under an argon atmosphere (50 kPa) and constant stirring using a magnetic stirrer. A Xe lamp (LA-251Xe, Hayashi Tokei) equipped with an optical filter (irradiated wavelength > 420 nm; Y-44, Hoya) and light-emitting diode (LED) lamps with wavelengths of 545 (LEDH60-545, Hamamatsu Photonics), 610 (LEDH60-600, Hamamatsu Photonics), 700 (LEDH60-700, Hamamatsu Photonics), and 740 nm (LEDH60-740, Hamamatsu Photonics) were used for light irradiation. The amount of evolved H_2 and O_2 was monitored using an online GC-8A gas chromatograph. AQE values were calculated using the amount of evolved O_2 in the same way as described above.

Photocatalytic overall water-splitting by $ZnRh_2O_4/Ag/s-Bi_4V_2O_{11}$ was also evaluated using pure water containing 33% isotopic water ($H_2^{18}O$, purity 97 atm% ^{18}O; Sigma-Aldrich) under light irradiation emitted from the 740 nm LED. The evolved gas was detected using

This journal is © the Owner Societies 2016

Phys. Chem. Chem. Phys., 2016, **18**, 27754–27760 | **27755**

a gas chromatograph/mass spectrometer (GC/MS; GCMS-QP 2010 Ultra, Shimadzu), which was operated in the selective-ion mode and monitored ions with masses of 28 ($^{14}N^{14}N$), 32 ($^{16}O^{16}O$), 34 ($^{18}O^{16}O$), and 36 ($^{18}O^{18}O$). The measurement conditions, other than those used for pure water containing isotropic water, were the same as those used in the photocatalytic overall pure-water splitting tests.

Results and discussion

Characterization

A back-reflection Laue pattern taken from normal to the plate surface of a $Bi_4V_2O_{11}$ single crystal is shown in Fig. S1 (ESI 2†). The distribution of diffraction spots revealed that $Bi_4V_2O_{11}$ was a single crystal. XRD patterns for a single crystal of $Bi_4V_2O_{11}$ and the powders obtained by pulverizing the single crystals of $Bi_4V_2O_{11}$ were also determined (Fig. 1). For the single $Bi_4V_2O_{11}$ crystal in the direction normal to the plate surface, only ($00l$) peaks were detected, indicating that the plate face of the single crystal corresponded to the (001) plane. This assumption is reasonable because $Bi_4V_2O_{11}$ is an Aurivillius-type bismuth layer-structured oxide (BLSO) and consists of alternating $(Bi_2O_2)^{2+}$ layers and oxygen-deficient pseudo-perovskite blocks of $(VO_{3.5}\square_{0.5})^{2-}$ along the c-axis.[31] Thus, because the growth rate of BLSO crystals in the c-axis direction is much lower than that along the $a(b)$-axis, single crystals of $Bi_4V_2O_{11}$ in the form of thin plate-like sheets with plate faces in the (001) plane were obtained. For the pulverized powder, all of the observed XRD peaks could be assigned to those for $Bi_4V_2O_{11}$. The BET surface areas of pulverized s-$Bi_4V_2O_{11}$ and as-prepared $ZnRh_2O_4$ powders were 0.179 and 3.60 $m^2 g^{-1}$, respectively.

UV-vis absorption and PA spectra of s-$Bi_4V_2O_{11}$ are shown in Fig. 2. Although the UV-vis absorption intensity decreased with increasing wavelength, relatively strong intensity was observed in longer wavelength regions. In contrast, the PA absorption of s-$Bi_4V_2O_{11}$ decreased with increasing wavelength, a property that reflects true photoabsorption,[30] which will be discussed later.

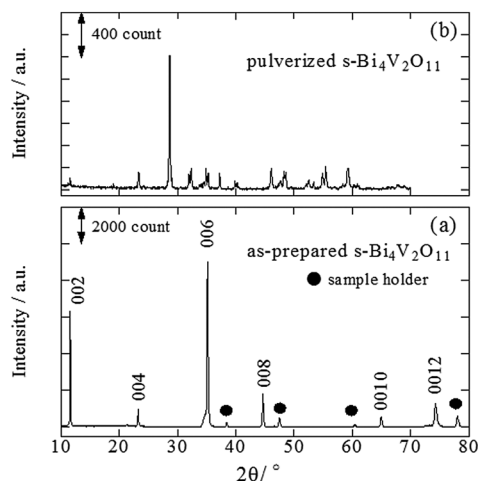Fig. 2 UV-visible absorption and PA spectra of s-$Bi_4V_2O_{11}$.

The XRD pattern of $ZnRh_2O_4$/Ag/s-$Bi_4V_2O_{11}$ following HNO$_3$ treatment is shown in Fig. 3. The XRD peaks mainly corresponded to two phases originating from $ZnRh_2O_4$ and $Bi_4V_2O_{11}$, although trace peaks attributable to a type of Ag oxide, such as AgVO$_3$, were also detected. However, Ag peaks were not observed. This result is plausible because most of the Ag was likely removed by the HNO$_3$ treatment and the amount of Ag remaining in the composite was below the limit of detection.

UV-vis absorption spectra of s-$Bi_4V_2O_{11}$, $ZnRh_2O_4$, and $ZnRh_2O_4$/Ag/s-$Bi_4V_2O_{11}$ with and without HNO$_3$ treatment are shown in Fig. 4. As can be seen in the spectra, untreated $ZnRh_2O_4$/Ag/s-$Bi_4V_2O_{11}$ showed greater absorption at wavelengths
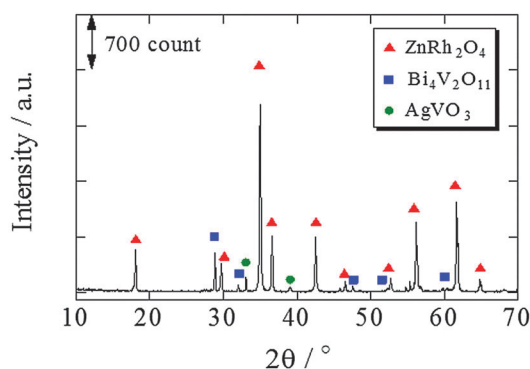
Fig. 3 XRD patterns of $ZnRh_2O_4$/Ag/s-$Bi_4V_2O_{11}$ after HNO$_3$ treatment.

Fig. 1 XRD patterns of the as-prepared (a) and pulverized s-$Bi_4V_2O_{11}$ (b).
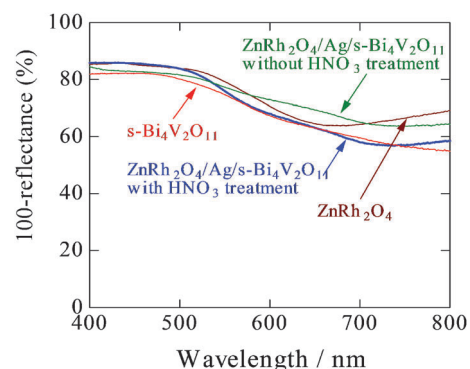
Fig. 4 UV-visible absorption spectra of s-$Bi_4V_2O_{11}$, $ZnRh_2O_4$, and $ZnRh_2O_4$/Ag/s-$Bi_4V_2O_{11}$ (with and without HNO$_3$ treatment).
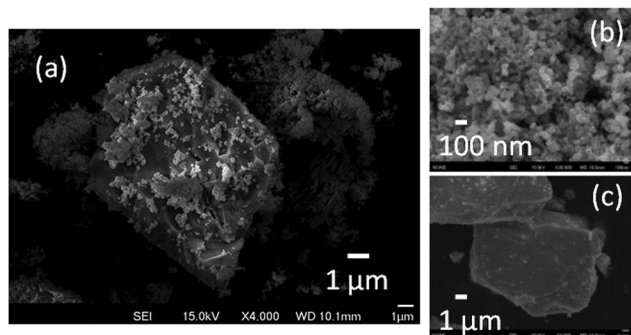
Fig. 5 SEM images of ZnRh$_2$O$_4$/Ag/s-Bi$_4$V$_2$O$_{11}$ powder after HNO$_3$ treatment (a), as-prepared ZnRh$_2$O$_4$ (b) and pulverized s-Bi$_4$V$_2$O$_{11}$ (c) powders.
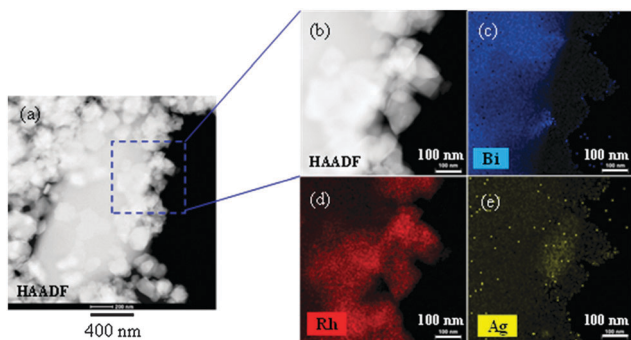
Fig. 6 STEM images of ZnRh$_2$O$_4$/Ag/s-Bi$_4$V$_2$O$_{11}$ after HNO$_3$ treatment. STEM image (a), its enlargement (b), and EDS element maps (c–e), in which blue (c), red (d), and yellow (e) colors correspond to Bi, Rh, and Ag, respectively.
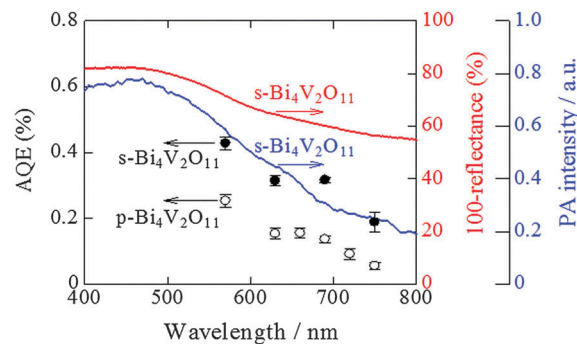

Fig. 7 Action spectra for O$_2$ evolution by the half reaction of water over s-Bi$_4$V$_2$O$_{11}$ (solid circles) and p-Bi$_4$V$_2$O$_{11}$ (open circles) in the presence of Ce^{4+}. The UV-visible absorption (red line) and PA (blue line) spectra of s-Bi$_4$V$_2$O$_{11}$ are also shown.

longer than ∼600 nm compared to HNO$_3$-treated ZnRh$_2$O$_4$/Ag/s-Bi$_4$V$_2$O$_{11}$. After the HNO$_3$ treatment, the absorption by ZnRh$_2$O$_4$/Ag/s-Bi$_4$V$_2$O$_{11}$ at wavelengths longer than ∼600 nm decreased and the spectral profile was in between those of ZnRh$_2$O$_4$ and s-Bi$_4$V$_2$O$_{11}$. Photos of pulverized s-Bi$_4$V$_2$O$_{11}$, as-prepared ZnRh$_2$O$_4$, and ZnRh$_2$O$_4$/Ag/p-Bi$_4$V$_2$O$_{11}$ after HNO$_3$ treatment are shown in Fig. S2 (ESI 3†).

In an SEM image of HNO$_3$-treated ZnRh$_2$O$_4$/Ag/s-Bi$_4$V$_2$O$_{11}$ powder, small ZnRh$_2$O$_4$ (∼50–100 nm) and large Bi$_4$V$_2$O$_{11}$ particles (∼10 μm) were clearly visible (Fig. 5a). Notably, the particle size of each photocatalytic material was identical to that before preparation of the heterojunction photocatalyst (Fig. 5b and c). STEM imaging and EDS-based elemental mapping of HNO$_3$-treated ZnRh$_2$O$_4$/Ag/Bi$_4$V$_2$O$_{11}$ were also performed (Fig. 6a–e). As was observed in the SEM image, the s-Bi$_4$V$_2$O$_{11}$ and ZnRh$_2$O$_4$ particles were clearly distinguishable (Fig. 6a and b) based on size differences. In addition, Ag was distributed (Fig. 6e) between the areas of Bi (Fig. 6c) and Rh (Fig. 6d), indicating that the Ag was inserted between the particles of ZnRh$_2$O$_4$ and Bi$_4$V$_2$O$_{11}$.

Action spectra for O$_2$ evolution of Bi$_4$V$_2$O$_{11}$

To examine and compare the activity of s-Bi$_4$V$_2$O$_{11}$ with that of p-Bi$_4$V$_2$O$_{11}$ as an O$_2$ evolution photocatalyst, the half reaction of water over s-Bi$_4$V$_2$O$_{11}$ and p-Bi$_4$V$_2$O$_{11}$ was evaluated using an

aqueous Ce(SO$_4$)$_2$ solution containing Ce^{4+} as the sacrificial agent (Fig. 7). Aqueous Ce(SO$_4$)$_2$ is yellowish and transparent, and absorbs visible light up to a wavelength of ∼550 nm. Thus, we irradiated s-Bi$_4$V$_2$O$_{11}$ and p-Bi$_4$V$_2$O$_{11}$ with light at wavelengths of longer than 570 nm and found that both materials were able to produce O$_2$ under visible light up to 750 nm. This property indicates that the maximum E_g value of Bi$_4$V$_2$O$_{11}$ was 1.65 eV. The AQE values of s-Bi$_4$V$_2$O$_{11}$ were ∼2–3-fold larger than those of p-Bi$_4$V$_2$O$_{11}$. As s-Bi$_4$V$_2$O$_{11}$ is considered to have higher crystallinity and anisotropy than p-Bi$_4$V$_2$O$_{11}$, photogenerated electrons and holes would therefore have enhanced mobility and separation (Fig. S3 in the ESI 4†).

It should be noted that the AQE values for O$_2$ evolution by s-Bi$_4$V$_2$O$_{11}$ were not consistent with the corresponding UV-vis absorption spectrum. A discrepancy between AQE values and absorption is frequently encountered, particularly for absorption in longer wavelength regions.[32,33] In contrast, the AQE values for O$_2$ evolution coincided well with the PA absorption spectrum, which is generally accepted as corresponding to true absorption.[30] Thus, it can be concluded that the O$_2$ evolution reaction proceeded via photoinduced band excitation (Fig. S3 in the ESI 4†). This excitation can be assigned to that originating from the VB, which contains O 2p and Bi 6s orbitals from the (Bi$_2$O$_2$)$^{2+}$ layers, to the CB, which is composed of a mixture of Bi 6p orbitals and antibonding O 2p and V 3d orbitals of (VO$_{3.5}$□$_{0.5}$)$^{2-}$ blocks.[34] The obtained E_g value (1.65 eV) is smaller than the previously reported values of ∼1.96–2.2 eV.[34–37] Although the reason for this difference is unclear, it may be attributable to the greater amount of oxygen defects in our samples (larger than 0.5 in VO$_{3.5}$□$_{0.5}$)$^{2-}$. The oxygen defect states form an isolated band below the CB bottom, whose width increases with the concentration of the defects, reaches the CB bottom, and finally starts to overlap with the CB, similar to the case of TiO$_2$.[38] In addition, it was reported that the band-gap of Bi$_4$V$_2$O$_{11}$ changes depending on the morphologies and preparation procedures.[37]

We previously reported that ZnRh$_2$O$_4$ can utilize visible light at wavelengths up to 770 nm and is also likely capable of utilizing infrared light for H$_2$ evolution.[32] Thus, ZnRh$_2$O$_4$/Ag/s-Bi$_4$V$_2$O$_{11}$ is expected to be sensitive to visible light up to at least 750 nm.

This journal is © the Owner Societies 2016

Phys. Chem. Chem. Phys., 2016, 18, 27754–27760 | 27757

Overall water splitting

The time courses of H_2 and O_2 evolution from pure water by $ZnRh_2O_4/Ag/s\text{-}Bi_4V_2O_{11}$ powder under visible-light irradiation (>420 nm) are shown in Fig. S4 (ESI 5†). Under these conditions, the linear generation of H_2 and O_2 at a molar ratio of 2 to 1 was observed. We performed this experiment with newly prepared powders and observed similar H_2 and O_2 evolution rates, confirming the reproducibility of the data. In addition, we characterized the prepared $ZnRh_2O_4/Ag/s\text{-}Bi_4V_2O_{11}$ powder after the water-splitting reaction under the same conditions as used in Fig. S4 (ESI†) by XRD and STEM/EDS and found that the sample did not appear to have changed (Fig. S5 and S6 in the ESI 5†). We also confirmed that the water-splitting reaction did not occur in the dark (data not shown).

The time courses of H_2 and O_2 evolution resulting from water splitting by $ZnRh_2O_4/Ag/s\text{-}Bi_4V_2O_{11}$ and $ZnRh_2O_4/Ag/p\text{-}Bi_4V_2O_{11}$ under irradiation with monochromic light with wavelengths of 545, 610, 700, and 740 nm were next measured (Fig. 8a–d). Under all conditions, $ZnRh_2O_4/Ag/s\text{-}Bi_4V_2O_{11}$ evolved H_2 and O_2 from water at a molar ratio of 2 to 1. The H_2 and O_2 evolution rates of $ZnRh_2O_4/Ag/s\text{-}Bi_4V_2O_{11}$ irradiated with 610 nm and 700 nm light were ~two- and three-fold larger, respectively, than those of $ZnRh_2O_4/Ag/p\text{-}Bi_4V_2O_{11}$. In addition, the induction period for linear H_2 and O_2 evolution was shortened. Upon irradiation with 740 nm light, $ZnRh_2O_4/Ag/s\text{-}Bi_4V_2O_{11}$ evolved H_2 and O_2 at a ratio of 2 to 1 after the induction period, whereas $ZnRh_2O_4/Ag/p\text{-}Bi_4V_2O_{11}$ only produced a trace amount of H_2. Thus, overall water splitting induced by 740 nm light was only achieved with $ZnRh_2O_4/Ag/s\text{-}Bi_4V_2O_{11}$ and was attributable to the enhanced O_2-evolution

Fig. 8 Time courses of H_2 and O_2 evolution resulting from water splitting by $ZnRh_2O_4/Ag/s\text{-}Bi_4V_2O_{11}$ (closed circles with solid lines) and $ZnRh_2O_4/Ag/p\text{-}Bi_4V_2O_{11}$ (open circles with broken lines) under irradiation with 545 nm LED (a), 610 nm LED (b), 700 nm LED (c), and 740 nm LED light (d). The H_2 and O_2 evolution data of $ZnRh_2O_4/Ag/p\text{-}Bi_4V_2O_{11}$ with 610 nm LED and 700 nm LED light are cited from ref. 27.

activity of $s\text{-}Bi_4V_2O_{11}$. Although the reason for the delay in H_2 and O_2 evolution is unclear, this phenomenon has been observed with other materials.[27] The delay might be due to existing defects,[39] redox reactions other than water-splitting reactions,[39–42] reconstruction of surface states,[43] or adsorption of H_2 and O_2 molecules on the photocatalyst surface.[43,44] However, the delay can be shortened by enhancing the activity.

As shown in Fig. 7, the AQE value of $s\text{-}Bi_4V_2O_{11}$ for O_2 was ~0.2% even at 750 nm and $s\text{-}Bi_4V_2O_{11}$ was expected to evolve O_2 under the entire range of visible light (~770 nm). Thus, further enhancement of O_2 evolution activity by $s\text{-}Bi_4V_2O_{11}$ would allow $ZnRh_2O_4/Ag/s\text{-}Bi_4V_2O_{11}$ to utilize the entire range of visible light and even near-infrared light, as the E_g value of $ZnRh_2O_4$ is 1.2 eV,[33] for the overall water-splitting.

The mechanisms of O_2 evolution on $BiVO_4$(010) and (011) facets were previously proposed.[45] On both surfaces, water molecules favorably adsorb on Bi sites. On the (010) surface, photogenerated holes induce the removal of two protons from the adsorbed water molecule in a stepwise manner, and the resulting O adatom obtains an electron by bonding with adjacent O anions to form a peroxo intermediate (Bi–O–O–V). Following the adsorption of a second water molecule at the same Bi site, a second O adatom is formed by the identical process and then obtains an electron from the nearby peroxo group, leading to the formation of a superoxo intermediate. A rapid rearrangement results in the formation of O_2, which is then desorbed from the surface. On the (010) surface, the V–O bond does not participate in the reaction, and a hydroperoxo intermediate (Bi–O–O–H) is formed after the adsorption of the second water molecule. Two protons are removed from the adsorbed water molecule in a stepwise manner, and O_2 is released from the surface. For both the (010) and (011) surfaces, it is likely that O_2 forms *via* peroxo species on $BiVO_4$, similar to the process that occurs on TiO_2.[46,47] In the case of $Bi_4V_2O_{11}$, because the VB is composed of hybrid O 2p and Bi 6s orbitals of the $(Bi_2O_2)^{2+}$ layers, the intermediate species would be the hydroperoxo group.

Fig. 9 shows the action spectrum for overall pure-water splitting by $ZnRh_2O_4/Ag/s\text{-}Bi_4V_2O_{11}$. We calculated the total number of incident photons from each LED light source and the O_2-evolution rates from the slopes of the plots in Fig. 8a–d and then estimated the AQE values (Table S1 in the ESI 6†). Because the H_2 and O_2 evolution rates were 2:1 for all wavelengths, the obtained AQE values for O_2 evolution were nearly identical to those for H_2 evolution. The shape of the action spectrum for overall water splitting by $ZnRh_2O_4/Ag/s\text{-}Bi_4V_2O_{11}$ was more similar to that of the PA spectrum of $s\text{-}Bi_4V_2O_{11}$ than that of the UV-vis absorption spectrum of $s\text{-}Bi_4V_2O_{11}$. An identical phenomenon was observed for the action spectrum of $s\text{-}Bi_4V_2O_{11}$ for O_2 evolution in aqueous Ce^{4+} solution (Fig. 7), indicating that the overall pure-water splitting reaction proceeded *via* the band-gap excitation of $s\text{-}Bi_4V_2O_{11}$, as well as $ZnRh_2O_4$, which has an E_g value of 1.2 eV, and can therefore absorb longer wavelength light than $s\text{-}Bi_4V_2O_{11}$. For this reason, the AQE values reflected the active photoabsorption capacity of $s\text{-}Bi_4V_2O_{11}$.

To confirm the liberation of O_2 from water by $ZnRh_2O_4/Ag/s\text{-}Bi_4V_2O_{11}$, water splitting with water containing 33% $H_2^{18}O$

27758 | *Phys. Chem. Chem. Phys.*, 2016, **18**, 27754–27760

This journal is © the Owner Societies 2016

Fig. 9 Action spectra for O_2 evolution from pure water by $ZnRh_2O_4$/Ag/s-$Bi_4V_2O_{11}$ (solid circles) and $ZnRh_2O_4$/Ag/p-$Bi_4V_2O_{11}$ (open circles) under irradiation with LED light sources. Note that the AQE values for H_2 evolution were almost identical to those for O_2 evolution, as H_2 and O_2 evolution at a ratio of 2 : 1 was observed. The UV–visible absorption (red line) and PA (blue line) spectra of s-$Bi_4V_2O_{11}$ are also shown. The AQE values of $ZnRh_2O_4$/Ag/p-$Bi_4V_2O_{11}$ irradiated with 610 nm and 700 nm LED are cited from ref. 27.

under irradiation with 740 nm light (740 nm LED, the same intensity in Fig. 8d) was next examined (Fig. 10). The amount of $^{16}O^{16}O$ (calc. $^{16}O^{16}O$) was obtained using the equation calc. $^{16}O^{16}O$ = obs. $^{16}O^{16}O$ − (obs. $^{14}N^{14}N$/0.78) × 0.21, because the detected $^{14}N^{14}N$ (N_2) originated from external air that entered the GC/MS system rather than from air dissolved in water, as was demonstrated in our previous report.[26,27] Under irradiation with 740 nm light for 120 h, $^{16}O^{16}O$, $^{16}O^{18}O$, and $^{18}O^{18}O$ were detected at a ratio of 4.00 : 3.97 : 1.03, which was close to the theoretical ratio of 4 : 4 : 1 for overall water-splitting. In addition, the time course of total O_2 evolution ($^{16}O^{16}O$ + $^{16}O^{18}O$ + $^{18}O^{18}O$) using water containing 33% $H_2^{18}O$ was consistent with that using normal $H_2^{16}O$ (solid circles with a solid line in Fig. 10, the same data as in Fig. 8d with the same symbol). Therefore, it was confirmed that O_2 was evolved from water by $ZnRh_2O_4$/Ag/s-$Bi_4V_2O_{11}$ under irradiation with 740 nm light. Based on these results, we confidently concluded that $ZnRh_2O_4$/Ag/s-$Bi_4V_2O_{11}$ was capable of overall pure-water splitting
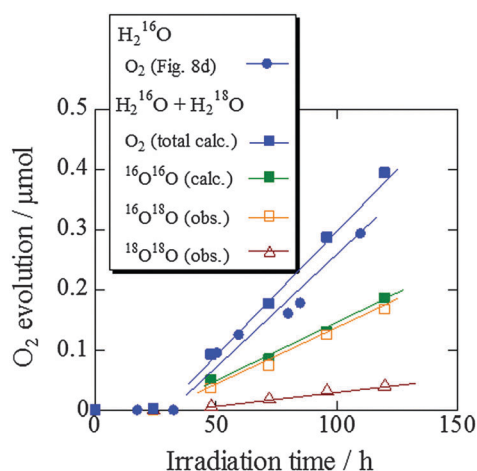
Fig. 10 GC/MS spectrometry results for the splitting of water containing 33% $H_2^{18}O$ by $ZnRh_2O_4$/Ag/s-$Bi_4V_2O_{11}$ irradiated with 740 nm LED light.

under visible-light irradiation with a wavelength of 740 nm (Scheme S1 in the ESI 7†).

In a previous study,[27] we attempted to scale up the overall pure-water splitting reaction by increasing the amounts of $ZnRh_2O_4$/Ag/p-$Bi_4V_2O_{11}$ and pure water by a factor of 10 (600 mg of photocatalyst was suspended in 120 mL pure water). Using this approach, the amounts of evolved H_2 and O_2 increased ∼40 fold, although the amounts of photocatalyst and water were increased only tenfold. Further improvements in the yields of H_2 and O_2 evolution may be possible by optimization of the ratio of the photocatalyst and water, modifying the shape and/or volume of the reaction vessel, how the light is irradiated, and other chemical engineering-based modifications.

Conclusions

We prepared the solid-state heterojunction photocatalyst $ZnRh_2O_4$/Ag/s-$Bi_4V_2O_{11}$ and demonstrated that this material simultaneously evolves H_2 and O_2 from pure water at a molar ratio of ∼2 to 1 under irradiation with nearly the entire range of visible light at wavelengths of up to 740 nm. Through the use of s-$Bi_4V_2O_{11}$ in place of p-$Bi_4V_2O_{11}$, the AQE for overall water splitting was increased and the sensitivity of the system was increased to wavelengths up to 740 nm. $ZnRh_2O_4$ was used as the H_2 photocatalyst in the present system because it has an E_g value of 1.2 eV and is therefore capable of effectively utilizing both visible and infrared light. Despite this desirable property, $ZnRh_2O_4$ is not suitable for large-scale systems because it contains Rh, which is a rare chemical element. Moreover, in this system, HNO_3 treatment is required for removing the excess Ag to achieve overall pure-water splitting, because Ag acts as a sacrificial agent for O_2 evolution. Such treatment might damage $ZnRh_2O_4$ and $Bi_4V_2O_{11}$, leading to decreased photocatalytic activity. To avoid such damage and potentially further improve the activity, we replaced Ag with gold (Au), because Au is stable and does not act as a sacrificial agent, and confirmed that an Au-inserted $ZnRh_2O_4$ and $Bi_4V_2O_{11}$ ($ZnRh_2O_4$/Au/s-$Bi_4V_2O_{11}$) system is capable of overall pure-water splitting. Detailed studies of $ZnRh_2O_4$/Au/s-$Bi_4V_2O_{11}$ are currently underway in our laboratory.

Acknowledgements

Notes and references

1 A. Fujishima and K. Honda, *Nature*, 1972, **238**, 37–38.
2 J. Sato, N. Saito, H. Nishiyama and Y. Inoue, *J. Phys. Chem. B*, 2001, **105**, 6061–6063.

This journal is © the Owner Societies 2016

Phys. Chem. Chem. Phys., 2016, **18**, 27754–27760 | 27759

3 K. Domen, A. Kudo, T. Onishi, N. Kosugi and H. Kuroda, *J. Phys. Chem.*, 1986, **90**, 292–295.

4 H. Kato, K. Asakusa and A. Kudo, *J. Am. Chem. Soc.*, 2003, **125**, 3082–3089.

5 K. Domen, J. Kondo, M. Hara and T. Takata, *Bull. Chem. Soc. Jpn.*, 2000, **73**, 1307–1331.

6 A. Kudo, *Int. J. Hydrogen Energy*, 2007, **32**, 2673–2678.

7 K. Maeda, R. Abe and K. Domen, *J. Phys. Chem. Lett.*, 2011, **115**, 3057–3064.

8 K. Maeda, K. Teramura, D. Lu, T. Takata, N. Saito, Y. Inoue and K. Domen, *Nature*, 2006, **440**, 295.

9 K. Maeda, T. Takata, M. Hara, N. Saito, Y. Inoue, H. Kobayashi and K. Domen, *J. Am. Chem. Soc.*, 2005, **127**, 8286–8287.

10 K. Maeda, K. Teramura, T. Takata, M. Hara, N. Saito, K. Toda, Y. Inoue, H. Kobayashi and K. Domen, *J. Phys. Chem. B*, 2005, **109**, 20504–20510.

11 K. Teramura, K. Maeda, T. Saito, T. Takata, N. Saito, Y. Inoue and K. Domen, *J. Phys. Chem. B*, 2005, **109**, 21915–21921.

12 Y. Lee, H. Terashima, Y. Shimodaira, K. Teramura, M. Hara, H. Kobayashi, K. Domen and M. Yashima, *J. Phys. Chem. C*, 2007, **111**, 1042–1048.

13 H. Liu, J. Yuan, W. Shangguan and Y. Teraoka, *J. Phys. Chem. C*, 2008, **112**, 8521–8523.

14 N. Lei, M. Tanabe and H. Irie, *Chem. Commun.*, 2013, **49**, 10094–10096.

15 P. Dhanasekaran and N. M. Gupta, *Int. J. Hydrogen Energy*, 2012, **37**, 4897–4907.

16 R. Asai, H. Nemoto, Q. Jia, K. Saito, A. Iwase and A. Kudo, *Chem. Commun.*, 2014, **50**, 2543–2546.

17 L. Liao, Q. Zhang, Z. Su, Z. Zhao, Y. Wang, Y. Li, X. Lu, D. Wei, G. Feng and Q. Yu, *et al.*, *Nat. Nanotechnol.*, 2014, **9**, 69–73.

18 C. Pan, T. Takata, M. Nakabayashi, T. Matsumoto, N. Shibata, Y. Ikuhara and K. Domen, *Angew. Chem., Int. Ed.*, 2015, **54**, 1–6.

19 J. Liu, Y. Liu, N. Liu, Y. Han, X. Zhang, H. Huang, Y. Lifshitz, S. T. Lee, J. Zhong and Z. Kang, *Science*, 2015, **347**, 970–974.

20 K. Sayama, K. Mukasa, R. Abe, Y. Abe and H. Arakawa, *J. Photochem. Photobiol., A*, 2002, **148**, 71–77.

21 H. Kato, Y. Sasaki, A. Iwase and A. Kudo, *Bull. Chem. Soc. Jpn.*, 2007, **80**, 2457–2464.

22 A. Kudo, *Pure Appl. Chem.*, 2007, **79**, 1917–1927.

23 S. Tanigawa and H. Irie, *Appl. Catal., B*, 2016, **180**, 1–5.

24 Y. Sasaki, H. Nemoto, K. Saito and A. Kudo, *J. Phys. Chem. C*, 2009, **113**, 17536–17542.

25 A. Iwase, Y. H. Ng, Y. Ishiguro, A. Kudo and R. Amal, *J. Am. Chem. Soc.*, 2011, **133**, 11054–11057.

26 R. Kobayashi, S. Tanigawa, T. Takashima, B. Ohtani and H. Irie, *J. Phys. Chem. C*, 2014, **118**, 22450–22456.

27 R. Kobayashi, K. Kurihara, T. Takashima, B. Ohtani and H. Irie, *J. Mater. Chem. A*, 2016, **4**, 3061–3067.

28 N. Yasuda, M. Miyayama and T. Kudo, *Mater. Res. Bull.*, 2001, **36**, 323–333.

29 N. Murakami, O. O. P. Mahaney, T. Torimoto and B. Ohtani, *Chem. Phys. Lett.*, 2006, **426**, 204–208.

30 N. Murakami, O. O. P. Mahaney, R. Abe, T. Torimoto and B. Ohtani, *J. Phys. Chem. C*, 2007, **111**, 11927–11935.

31 G. Mairesse, P. Roussel, R. N. Vannier, M. Anne, C. Pirovano and G. Nowogrocki, *Solid State Sci.*, 2003, **5**, 851–859.

32 H. Irie, Y. Watanabe and K. Hashimoto, *J. Phys. Chem. B*, 2003, **107**, 5483–5486.

33 Y. Takimoto, T. Kitta and H. Irie, *Int. J. Hydrogen Energy*, 2012, **37**, 134–138.

34 Y. Lu, Y. Pu, J. Wang, C. Qin, C. Chen and H. J. Seo, *Appl. Surf. Sci.*, 2015, **347**, 719–726.

35 V. Thakral and S. Uma, *Mater. Res. Bull.*, 2010, **45**, 1250–1254.

36 S. Kumar and P. D. Sahare, *NANO: Brief Rep. Rev.*, 2013, **8**, 1350007.

37 X. Chen, J. Liu, H. Wang, Y. Ding, Y. Sun and H. Yan, *J. Mater. Chem. A*, 2013, **1**, 877–883.

38 I. Justicia, P. Ordejon, G. Canto, J. L. Mozos, J. Fraxedas, G. A. Battiston, R. Gerbasi and A. Figueras, *Adv. Mater.*, 2002, **14**, 1399–1402.

39 T. Ishii, H. Kato and A. Kudo, *J. Photochem. Photobiol., A*, 2004, **163**, 181–186.

40 R. Konta, T. Ishii, H. Kato and A. Kudo, *J. Phys. Chem. B*, 2004, **108**, 8992–8995.

41 H. W. Kang, S. N. Lim and S. B. Park, *Int. J. Hydrogen Energy*, 2012, **37**, 4026–4035.

42 H. W. Kang and S. B. Park, *Mater. Sci. Eng., B*, 2016, **211**, 67–74.

43 T. Uchihara, M. Matsumura, A. Yamamoto and H. Tsubimura, *J. Phys. Chem.*, 1989, **93**, 5870–5874.

44 J. F. Gomes, C. A. Martins, M. J. Giz, G. Tremiliosi-Filho and G. A. Camera, *J. Catal.*, 2013, **301**, 154–161.

45 J. Yang, D. Wang, X. Zhou and C. Li, *Chem. – Eur. J.*, 2013, **19**, 1320–1326.

46 T. Kisumi, A. Tsujiko, K. Murakoshi and Y. Nakato, *J. Electroanal. Chem.*, 2003, **545**, 99–107.

47 R. Nakamura and Y. Nakato, *J. Am. Chem. Soc.*, 2014, **126**, 1290–1298.

27760 | *Phys. Chem. Chem. Phys.*, 2016, **18**, 27754–27760

This journal is © the Owner Societies 2016